JOURNAL OF MATERIALS SCIENCE 30 (1995) 2008–2018

Parametric study of the plasma synthesis of ultrafine silicon nitride powders

G. SOUCY, J. W. JUREWICZ, M. I. BOULOS
Plasma Technology Research Centre (CRTP), Department of Chemical Engineering, Université de Sherbrooke, Sherbrooke, Québec, Canada, J1K 2R1

The high-temperature plasma synthesis of ultrafine silicon nitride (Si_3N_4) powders through the vapour-phase reaction between $SiCl_4$ and NH_3 in an Ar/H_2 radio frequency (r.f.) inductively coupled plasma was investigated. The experiments were carried out at a 25–39 kW plate power level and at atmospheric pressure. Special attention was paid to the influence of the reactor wall temperature and plasma operating conditions on the quality of the powder. With a cold-wall reactor, the powders obtained were white to light brown in colour and were composed of crystalline, amorphous and Si_3N_4 whisker phases. Both α and β-Si_3N_4 were present in these products. The NH_4Cl, formed as a by-product of the reaction, could be eliminated from the Si_3N_4 by thermal treatment. The BET specific surface area of the powder after thermal treatment was about 60 $m^2 g^{-1}$. The use of the hot-wall reactor resulted in a considerable reduction in the amount of NH_4Cl remaining in the powder (less than 1 wt%) and a considerable increase in the fraction of the powder obtained in crystalline form. These powders were composed of a mixture of amorphous phase and 30 wt% or more of the α and β–Si_3N_4 crystalline phases. The BET specific surface area of the powder after thermal treatment was found to be 40 $m^2 g^{-1}$. The experimental results are discussed in relation to their use for optimizing reactor design for the vapour-phase synthesis of ultrafine ceramic powders.

1. Introduction

There has been growing interest in structural ceramics over the past ten years. This is largely motivated by the need for high-performance structured materials for the aerospace and automotive industries [1, 2]. Silicon carbide and silicon nitride are among the top candidate materials which have been the subject of considerable study [3]. A number of processes have been developed for the synthesis of these two ceramics using a wide range of technologies. The following chemical routes are successfully used for these processes:

(i) direct nitridation of elemental silicon

$$3Si + 2N_2 \rightarrow Si_3N_4 \quad (1)$$

(ii) carbothermic reduction of silica

$$3SiO_2 + 2N_2 + 6C \xrightarrow{1573-1973\,K} Si_3N_4 + 6CO \quad (2)$$

(iii) pyrolysis of $Si(NH)_2$

$$3SiCl_4 + 16NH_3 \xrightarrow{1573-1973\,K} 3Si(NH)_2 + 12NH_4Cl \quad (3a)$$

$$3Si(NH)_2 \xrightarrow[1373-1873\,K]{} Si_3N_4 + 2NH_3 \quad (3b)$$

(iv) gas-phase reaction

$$3SiCl_4 + 4NH_3 \xrightarrow{1373-1623\,K} Si_3N_4 + 12HCl \quad (4a)$$

$$HCl + NH_3 \rightarrow NH_4Cl \quad (4b)$$

The direct nitridation of elemental silicon [4] is widely used because of its relative simplicity and low cost. Si_3N_4 can be prepared according to this route by heating elemental silicon in a nitrogen atmosphere at 1573–1773 K for a few hours. This solid–gas reaction phase is exothermic and difficult to control in terms of the particle shape and size of the powder obtained and its phase content. The kinetics of this reaction are, however, relatively slow [5] and the process often requires the addition of a catalyst (iron). This path also requires many steps during the synthesis process which can affect the purity of the product.

The carbothermic reduction of the silica [6] has the same limitations as the direct nitridation of elemental silicon and is complicated by the numerous reaction steps and simultaneous formation of co-products silicon oxynitride (Si_2N_2O) and silicon carbide (SiC).

The pyrolysis of $Si(NH)_2$ has been used over the recent decade to prepare pure α-Si_3N_4 via a relatively simple liquid-phase process, often identified as the Japanese UBE process [7]. The principal limitations

0022–2461

are the need for post-synthesis heat treatment to obtain the crystalline form of the powder and the risk of powder contamination by the organic solvent used during the synthesis.

The thermal plasma route for the synthesis of silicon nitride (Si_3N_4) through the vapour-phase reaction is particularly attractive because of its ability to maintain a high degree of purity of both the reactants and the powder subsequently obtained. A summary of the process conditions examined by various investigators for the plasma synthesis of Si_3N_4 powder, using induction plasma technologies, are presented in Table I. The powders obtained in most of these studies were generally of high purity and had a particle in the size range 5–100 nm. A comparison of typical impurity levels found in the powders, produced by the different reaction routes is set out in Table II. The plasma-produced powders generally required a post-treatment step in order to remove any NH_4Cl co-condensed with the powder, in the case of the $SiCl_4 + NH_3$ route, and to improve the crystalisation, since most of the powder products were obtained in the amorphous state.

It is to the elimination of this process step that this investigation was devoted. Particular attention was paid to the details of the reactor design used which was developed to permit operation with hot-wall conditions in the powder condensation section. The powder characteristics obtained with this configuration are compared with those prepared using a standard cold-wall reactor.

2. Equilibrium calculations

In order to establish a theoretical basis for the gas-phase reaction system utilized in the plasma route, thermodynamic equilibrium calculations were carried out as the first stage of this investigation. The thermodynamic equilibrium compositions were calculated for the (Ar–Si–N–Cl–H) system, using the standard Gibbs free-energy minimization scheme [17] over the temperature range 300–4000 K. Based on some preliminary calculations, the following reactant species (30) were used in the computations: NH_3, NH_2, NH, N_2, N, H_2, H, Si_3, Si_2, Si, $Si_{(c)}$, SiH_4, SiH_3, SiH_2, SiH, SiCl, $SiCl_2$, $SiCl_3$, $SiCl_4$, SiH_2Cl, SiH_3Cl, $SiHCl_3$, NSi, NSi_2, a-$Si_3N_{4(s)}$, $NH_4Cl_{(s)}$, Cl_2, Cl, HCl, Ar. Values for Gibbs free energies of the different species were taken from JANAF's tables [18] except for SiH_3 and SiH_2 which were provided by Coltrin [19]. It may

TABLE I Overview of works on Si_3N_4 powder synthesis using induction plasma technology at atmospheric pressure

Conditions	Husain and Ibberson [11]	Li and Cu [12]	Szépvölgyi *et al.* [13]	Yoshida *et al.* [14]	Lee *et al.* [15]	Sheppard [16]
Reactants flowrate:						
$SiCl_4$ (g min^{-1})	3	33.6	< 0.8	< 3.1	< 3	n.a.[a]
NH_3 (standard l min^{-1})	10	< 166	< 4.8	20	< 5	< 20
Wall	Cold	Cold	Cold	Pyrex tube	Pyrex tube	613 K
Power (kW)	4–8	< 100	2.9–3.8	13–14	18–20	< 70
Frequency (MHz)	n.a.	3.6	27.17	5	5	4
Powder colour	Si: cream $SiCl_4$: white	White	White	White	White, cream	White
Structure	Amorphous	Amorphous	Amorphous	Amorphous	Amorphous, < 30% α-Si_3N_4	Amorphous
d_p (nm)	5–10	< 100	20–100	10–30	10–30	15
BET (m^2 g^{-1})	n.a.	> 40	33	n.a.	n.a.	n.a

[a] n.a. = not available.

TABLE II Summary of typical contaminant levels depending on the reaction routes

Contaminants	Direct nitridation of elemental silicon [8] (p.p.m.)	Carbothermic reduction of silica [5, 6] (p.p.m.)	Pyrolysis of $Si(NH)_2$ [9] (p.p.m.)	Gas-phase reaction [10] (p.p.m.)
Fe	29	110	50	16
Al	54	960	10	18
Ca	23	120	10	2
O	8600	22550	n.a.	10000
Cl	n.a.[a]	n.a.	3000	< 100
SiO_2	n.a.	17700	n.a.	n.a.
C	n.a.	6700	1000	n.a.

[a] n.a. = not available.

be noted that only data for α-$Si_3N_{4(s)}$ is included, because for β-$Si_3N_{4(s)}$ the Gibbs free energy is close to that of the α-phase, and accordingly cannot, be distinguished on the equilibrium diagram.

Computations were carried out for reaction mixtures (molar) composed of: 0.4 Ar + 0.02 H_2 + 0.06 $SiCl_4$ + xNH_3. Stoichiometric ratios of $NH_3/SiCl_4$ = 1.0; 1.23; 3.37; 5.0; 6.67; 10.0; 20.0; 50.0 were considered. Typical results obtained for the $NH_3/SiCl_4$ molar ratio of 6.67, over the temperature range 300–4000 K, are plotted as shown in Fig. 1. This plot shows that silicon nitride is a very stable compound below its sublimation temperature (2173 K). NH_4Cl is formed only at temperatures below 600 K while between 600 and 1800 K, α-$Si_3N_{4(s)}$ is the predominant solid species. Fig. 2 shows that the formation of α-$Si_3N_{4(s)}$ is optimum at around a $NH_3/SiCl_4$ molar ratio of 6.67. At higher $NH_3/SiCl_4$ NH_4Cl formation is favoured over that of α-$Si_3N_{4(s)}$, while at sub-stoichiometric $NH_3/SiCl_4$ values, the overall conversion to Si_3N_4 is reduced. Computations were repeated for the case of the absence of hydrogen in the plasma gas for a reaction mixture of 0.4 Ar + 0.06 $SiCl_4$ + 0.4 NH_3 over the same temperature range. The results, given in Fig. 3, show that the presence of hydrogen has virtually no influence on the mass fraction of the principal components in the equilibrium composition.

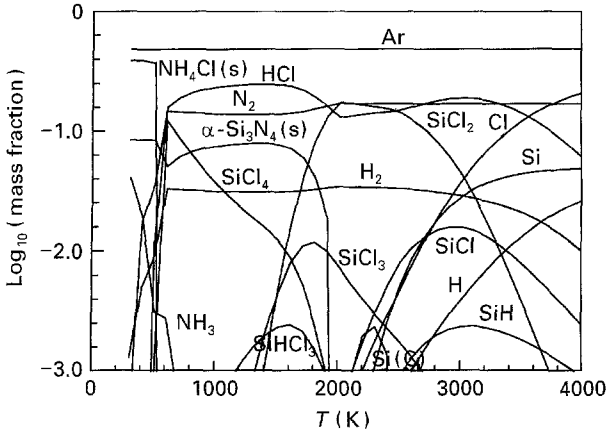

Figure 1 Equilibrium composition at atmospheric pressure for stoichiometric mixture ($NH_3/SiCl_4$ = 6.67) (0.4 Ar + 0.02H_2 + 0.06 $SiCl_4$ + 0.4 NH_3).

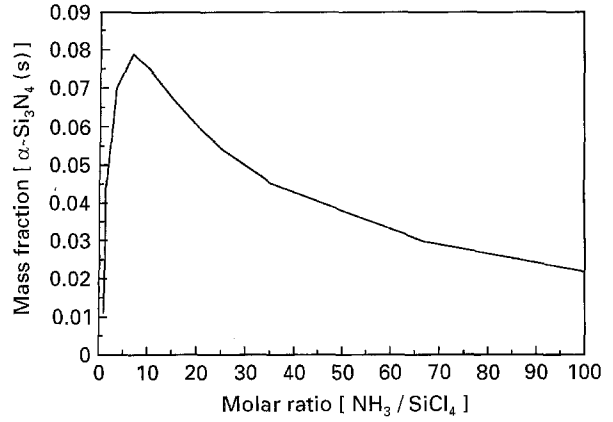

Figure 2 Variation of Si_3N_4 mass fraction versus the $NH_3/SiCl_4$ molar ratio at 1300 K and P = 1 atm for a reaction mixture of (0.4 Ar + 0.02 H_2 + 0.06 $SiCl_4$ + xNH_3).

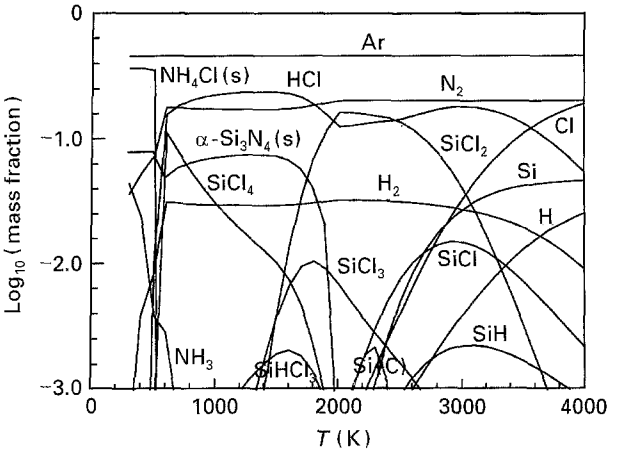

Figure 3 Equilibrium composition at atmospheric pressure for the stoichiometric mixture ($NH_3/SiCl_4$ = 6.67) in the absence of hydrogen in the plasma gas (0.4 Ar + 0.06 $SiCl_4$ + 0.4 NH_3).

3. Experimental procedure

Two experimental set-ups were used in this investigation in order to determine the effect of the reactor design on the morphology and crystal structure of the powder product. Both reactors used the same reactant systems ($SiCl_4$ + NH_3) in which the $SiCl_4$ vapours were injected axially in the centre of the discharge while ammonia was injected through a three-hole flange at the level of the exit nozzle of the torch. These features are shown in Fig. 4 a and b which corresponds to the cold- and hot-wall reactors, respectively. The principal sections for both reactor configurations are described below.

3.1. Induction plasma torch

The r.f. induction plasma torch used is of standard design, equipped with a water-cooled quartz, plasma confinement tube (50 mm i.d., 55 mm o.d.). In the hot-wall reactor condition, the quartz tube was replaced by a ceramic tube which features higher resistance to thermal shock. The magnetic field is provided by a five-turn induction coil. The torch is connected to a 50 kW Lepel r.f. power supply with an oscillator frequency of 3 MHz. The torch is operated with either Ar/H_2 mixtures or pure nitrogen as the sheath gas. Pure argon only is used as the central plasma gas. $SiCl_4$ is fed axially into the discharge using a water-cooled stainless steel probe while NH_3 is injected radially inwards at the exit of the plasma torch through an appropriate water-cooled stainless steel flange. The three, 1.0 mm i.d., NH_3 injection ports were oriented in the upstream direction at 45° to the torch axis. It is important to mention that this choice of the design for the NH_3 injection flange was supported by a systematic study on the mixing pattern in the torch/reactor system [20–22]. The results of this study showed that this configuration allows for faster reactant mixing without the need to locate the injec-

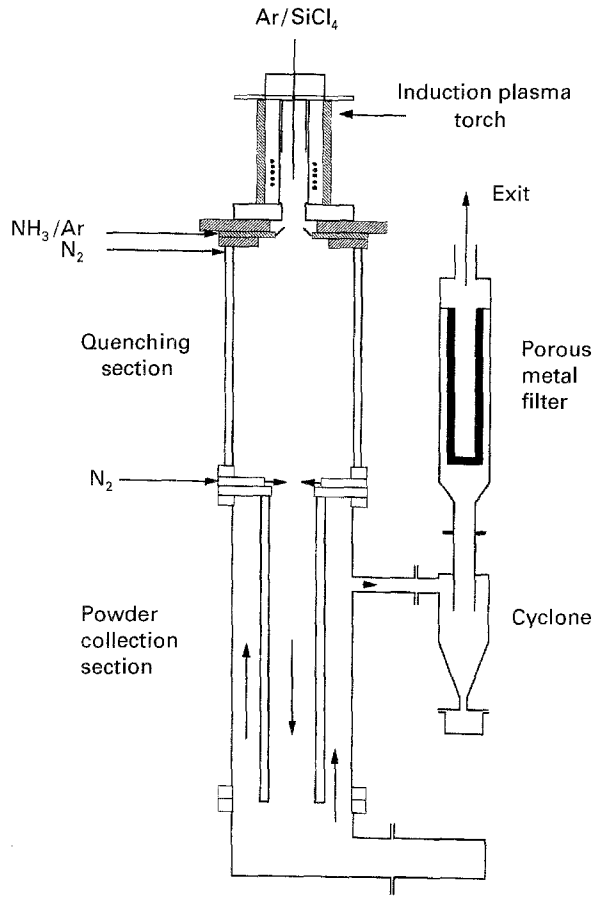

(a)

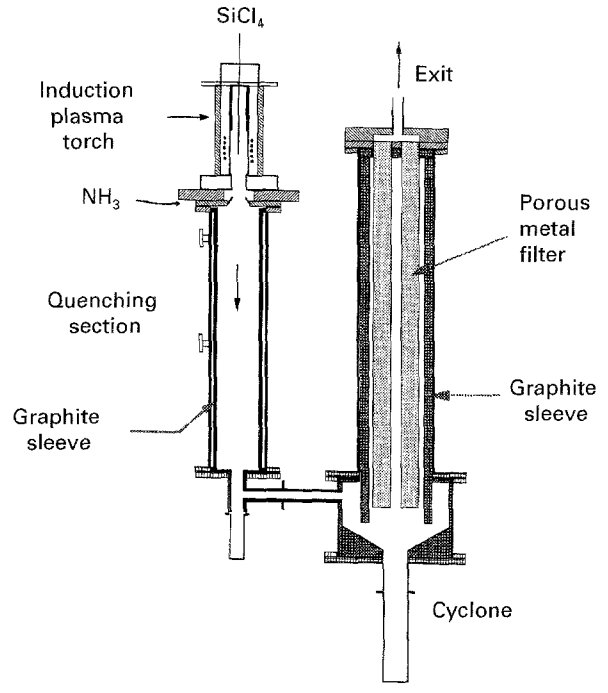

(b)

Figure 4 Schematic drawing of the experimental apparatus: (a) cold-wall reactor; (b) hot-wall reactor.

tion ports right into the exit nozzle of the plasma torch. Also for this configuration, radial injection velocities above 50 $m^{-1}s$ are necessary to obtain good penetration of the reactant gas which can be achieved by large NH_3 flowrate (> 30 standard l min^{-1}).

3.2. Reactor system

The cold-wall induction plasma reactor consists of a water-cooled, stainless steel cylindrical chamber (127 mm i.d., 737 mm long), named the product quenching module. A quenching gas injection flange was placed at both extremities. The product collection system consists of a water-cooled condensation section, followed by a cyclone and one unit of a 10 μm porous metal filter (38 mm diameter and 385 mm long). The absolute pressure in the reactor system was regulated by a throttle valve connected to a water-ring vaccum pump which also acted as a scrubber for gas cleaning before the exhaust gases were discharged into the atmosphere. More details can be found in the thesis of Soucy [23].

In contrast, in the hot-wall reactor study, the reactor system (Fig. 4b) was lined with a graphite sleeve inside the water-cooled, stainless steel cylindrical chamber. In the quench section, a graphite sleeve (80 mm i.d., 104 mm o.d. and 500 mm long) was used. To be able to run the plasma reactor for about 15 min without incurring blockage of the filter unit, the filtration area was increased by using three parallel units of Inconel 600, 5 μm porous metal filter (50 mm diameter and 760 mm long). This section was also covered by a graphite sleeve. Finally, the water-cooled condensation section was placed downstream of the filtration section to trap the NH_4Cl product. The graphite sleeves were preheated for 15 min prior to conducting each run, in order to ensure that the wall temperature near to the NH_3 injection port was higher than 673 K. The wall temperature was monitored by means of a radiation pyrometer sighted through a quartz window, located 15 cm below the exit of the torch. Wall temperatures reached in the reactor zone were confirmed using a "K" thermocouple only when the plasma was switched off because of the induced electromagnetic noise. In the filtration section, the temperatures indicated by bimetal thermometers, rose to only around 400 K because of the large available cooling surface. Some small cold regions remained close to the injection ports because it was impossible to protect them totally by the graphite sleeves.

3.3. $SiCl_4$ and NH_3 feeding system

Owing to the extremely corrosive nature of $SiCl_4$ and its sensitivity to oxidation as soon as it is exposed to air, special care had to be exercised to keep it, at all times, under an inert atmosphere. The best means for feeding $SiCl_4$ was found to be an eight-roller peristaltic pump. VITON pump tubes were necessary to resist the corrosion of $SiCl_4$. The $SiCl_4$ feed was evaporated by passing it through a stainless steel coil, 5.1 mm i.d. 1.5 m long, immersed in a well-agitated, constant temperature silicone oil bath maintained at 150 °C. At the exit of the vaporizer, the $SiCl_4$ feed was diluted with argon flow, preheated to the same temperature, using a second stainless steel coil immersed in the same oil bath. The $Ar/SiCl_4$ gas mixture was then transported to the injection probe in the induction plasma torch using an electrically heated stainless steel tube, 3 m long.

While stainless steel rotameters were satisfactory to monitor the NH_3 feed, our concern with the need for close control on the material balances justified the addition of a second NH_3 feed monitoring system, achieved by placing the NH_3 cylinder on an appropriate electronic balance. This provided us with accurate indication of the total NH_3 mass fed to the system for each reaction run.

3.4. Plasma operating conditions

Throughout this study the reactor configuration for both cold- and hot-wall conditions and the associated plasma operating conditions were kept essentially constant, exceptions being the plasma sheath gas (composition and flow rate) and the plasma plate power, both of which were varied over a limited range. A summary of the plasma operating conditions used in both wall conditions is provided in Table III. In the cold-wall reactor work, many parameters were studied, while the hot-wall reactor was used mainly to evaluate its effect on the chemical reactions and to compare the results obtained with cold-wall conditions.

3.5. Powder characterization

Considerable importance was attached to conducting extensive characterization, i.e. determining the physical and chemical nature of the powders obtained. The analyses were performed on the powders from which the NH_4Cl has been removed by thermal treatment, allowing the evaluation of NH_4Cl content for the powder of each run. The thermal treatment of the product consisted in heating the powders in an inert atmosphere argon to a temperature of 673 K for 5 h. The powder characterization techniques then applied were principally BET specific surface area measurement, X ray diffraction (XRD) analysis, Fourier transform–infrared (FT–IR) analysis, transmission electron microscopy (TEM), and energy dispersive spectroscopy (EDS). All the details of these techniques may be found in the thesis of Soucy [23], only the experimental results from the application of these techniques to the powder products are presented here.

4. Results and discussion

4.1. Cold-wall conditions

A total of 12 runs was carried out at plasma plate powers of 26–27 kW in which the principal parameter investigated was the $SiCl_4$ feed rate, which was varied over the range 2.4–18.5 g min^{-1}. As the NH_3 feed rate was kept essentially constant, the corresponding $NH_3/SiCl_4$ mixture molar ratio varied from 8–89. This covered essentially the range from a stoichiometric mixture to one in which the NH_3 concentration was in large excess. The experimental concept of the cold-wall condition was also aimed at determining the effect of (a) product quench gas (nitrogen), (b) variation in the plasma sheath gas composition and flow rate, (c) the plasma plate power and (d) the axial location of the $SiCl_4$ injection probe. A summary of the operating conditions and the physical characteristics of the powders obtained in cold-wall reaction condition is given in Table IV.

The products obtained in each of these runs were fluffy ultrafine powders, ranging in colour between white and brown. It was determined that the thermal treatment had no effect on the structure of the powder obtained. Depending on the operating conditions, the NH_4Cl content of the produced powders varied from 8.7 to 81.1% by weight. The powder collected in the reactor (R) generally showed a higher NH_4Cl content than that from the filter (F). The BET specific surface area was around 60 $m^2 g^{-1}$. In the case of the amorphous powder, the FT–IR analysis confirmed the presence of the Si–N bonds at 900 cm^{-1} wavelength.

4.1.1. Effect of $NH_3/SiCl_4$ ratio

In this experiment, runs C1–C5 were carried out in order to determine the effect of changes in the molar ratios of the reactants on the Si_3N_4 powder characteristics. These runs demonstrated that, as expected, the free NH_4Cl content of the powder increased with increase in the $NH_3/SiCl_4$ molar ratio. The NH_4Cl content reaches a plateau, however, at around a $NH_3/SiCl_4$ molar ratio of 60, beyond which the

TABLE III Summary of plasma operating conditions for cold- and hot-wall reactors

Parameters	Cold-wall reactor	Hot-wall reactor
Sheath gas (standard l min^{-1})	90.0–108.0 (Ar) + 6.2 (H_2) or 108.0 (N_2)	89.0 (Ar) + 9.6 (H_2)
Central gas (standard l min^{-1})	40.0 (Ar)	59.0 (Ar)
Diluent gas $SiCl_4$ (standard l min^{-1})	2.4 (Ar)	2.3 (Ar)
Diluent gas NH_3 (standard l min^{-1})	5.0 (Ar)	5.0 (Ar) (run H10 only)
Quench gas (standard l min^{-1})	40.0 (N_2) except no gas for run C6	none
Plate power (kW)	26.0–39.0	25.9–35.9
$SiCl_4$ injection position	78 mm above torch outlet except for run C12, at 68 mm	83 mm above torch outlet except for runs H1 and H2, at 78 mm

TABLE IV Summary of the experimental conditions related to the physical characteristics of the powders obtained from cold-wall configuration

Run	Gas flowrates		Plate power (KW)	feed rate $SiCl_4$ (g min^{-1})	feed rate NH_3 (g min^{-1})	$NH_3/SiCl_4$ molar ratio (m g^{-4})	Collected powder colour (nm)	NH_4Cl (wt %)	Crystal structure	BET specific surface (m^2 g^{-1})	TEM diameter (nm)
	Sheath (standard l min^{-1})	Quench (standard l min^{-1})									
C1-R	90 Ar + 6.2 H_2	40 N_2	26.5	2.4	21.1	89	White	67.5	Amorphous	43.1	25
F							White	58.8		63.3	22
C2-R	90 Ar + 6.2 H_2	40 N_2	27.6	4.0	23.0	59	White	81.1	Amorphous	63.0	36
F							White	54.0		64.6	22
C3-R	90 Ar + 6.2 H_2	40 N_2	27.6	9.0	22.6	25	White	51.8	Amorphous	60.8	38
F							White	23.3	$+\alpha+\beta$	63.2	55
C4-R	90 Ar + 6.2 H_2	40 N_2	27.6	17.5	20.8	12	Cream	35.2	Amorphous	59.9	27 and 46
F							Cream	8.7	$+\alpha+\beta$	58.4	28 and 46
C5-R	90 Ar + 6.2 H_2	40 N_2	26.8	17.0	13.6	8	Brown	35.0	Polymer	67.9	Agglom.
F							Brown	18.9	deposit	81.8	Agglom.
C6-R	90 Ar + 6.2 H_2	No gas	27.2	16.7	23.1	14	Cream	26.7	Amorphous	61.2	44
F							Cream	14.4	$+\alpha+\beta$	60.4	49
C7-R	90 Ar + 6.2 H_2	40 N_2	27.2	16.3	23.1	13	Cream	18.9	Amorphous	58.0	55
F							Cream	9.4	$+\alpha+\beta$	86.4	30
C8-R	90 Ar + 6.2 H_2	40 N_2	38.7	15.7	21.1	13.5	Brown	34.3	Polymer	57.4	Agglom.
F							Brown	85.7	deposit	76.9	Agglom.
C9-R	108N_2	40 N_2	27.7	16.2	20.9	13	White	44.7	Amorphous	54.0	27
F							White	33.7	$+\alpha$	56.0	22 and 49
C10-R	108 N_2 + 6.2 H_2	40 N_2	27.4	16.4	21.1	13	White	74.6	Amorphous	95.4	38
F							White	47.9	$+\alpha$	117.5	41
C11-R	90 Ar + 6.2 H_2	40 N_2	26.4	16.1	21.4	13	White	78.4	Amorphous	72.3	30
F							White	50.3	$+\alpha$	67.7	17 and 34
C12-R	90 Ar + 6.2 H_2	40 N_2	26.4	18.5	21.9	13	White	79.7	Amorpous	82.0	12 and 38
F							White	55.6	$+\alpha$	77.9	[a]

[a] No measurements.

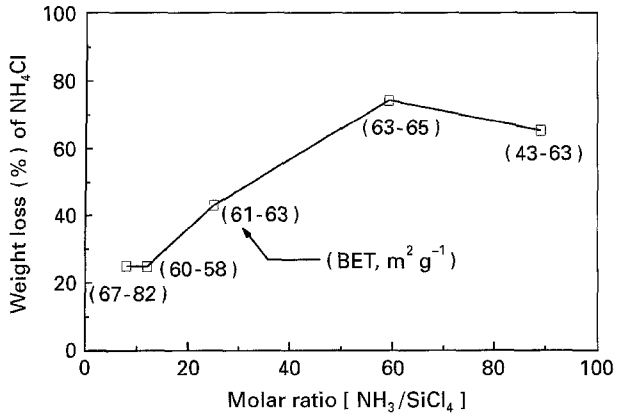

Figure 5 Molar ratio of $NH_3/SiCl_4$ versus weight loss (%) of NH_4Cl.

NH_4Cl content of the powder remained essentially constant. This indicates that complete conversion of the $SiCl_4$ and reaction product HCl to Si_3N_4 and NH_4Cl, respectively, had occurred according to the gas-phase reaction. The results are presented in Fig. 5, which also shows that the BET specific surface area of the powder remained constant at around 60–65 $m^2 g^{-1}$ with an increase of the $NH_3/SiCl_4$ molar ratio.

It is interesting to note, as recorded in Table IV, that the decrease in the NH_3 feed rate to below 20 $g m^{-1}$ resulted in a major change of the characteristics of the product from a fluffy white, or off-white, powder to a brown polymer-type deposit which was rather difficult to characterize. This change seems to be related to the gas mixing pattern established in the reactor, because the reduction in the NH_3 gas feed rate resulted in a corresponding decrease in the gas injection velocity at the exit of the plasma torch. This effect is reproduced at a higher NH_3 feed rate at high plasma power level (run C8) which could equally reflect mixing problems in the reactor under these conditions. This explanation is confirmed by the experimental mixing study [22], in which it was observed that the radial injection gas mass flowrate should be around 23 $g min^{-1}$ to obtain a high penetration of the NH_3 stream. This condition allows a longer contact time between $SiCl_4$ and NH_3. This is the reason why, in the hot-wall condition work, this high mass NH_3 feed rate was used.

4.1.2. Effect of plasma plate power

The experiment with the higher plasma plate power (run C8) confirmed the findings of Phillips and Vogt [24] regarding the strong effect of the reaction temperature on the synthesis process. The latter needs to be carried out over a rather narrow temperature range to provide the optimal conversion yield. To cope with that problem, the reactor design used should provide means for adjusting the relative/positional level at which the NH_3 is injected into the plasma gases flow to react with dissociated $SiCl_4$. This optimal position depends on the $SiCl_4$ point of injection and the plasma operating conditions.

4.1.3. Effect of product quench gas

The influence of the quench conditions on the synthesis reaction has also been studied (runs C6 and C7). It was found that if the hot stream of gases was quenched too fast, amorphous powder formation was favoured. The optimum reactor design should, therefore, encourage a longer residence time for the products in the high-temperature zone. It should also provide means for keeping the wall temperature of the condensation zone at or above 573 K, in order to avoid the co-condensation of solid NH_4Cl. A more crystalline product may also be obtained by maintaining a low $NH_3/SiCl_4$ molar ratio (10) to minimize the formation of NH_4Cl.

4.1.4. Effect of plasma sheath gas composition

The influence of nitrogen instead of argon injected as the sheath gas has also been investigated (runs C9 and C10). It was found that replacing the previously employed $Ar–H_2$ mixture by $N_2–H_2$ mixture at constant plate power, promotes the formation of amorphous powders. This result can be explained by possible changes in the plasma temperature profile, especially at its periphery. The run without hydrogen demonstrated that the pressure of H_2 favours slightly the formation of NH_4Cl.

4.1.5. Effect of $SiCl_4$ feed probe position

Runs C11 and C12 differed essentially only in the location of the axial point of injection of the $SiCl_4$ vapour into the plasma. The results indicate that a 10 mm shift in the $SiCl_4$ feed probe position had relatively little influence on the properties of the powders obtained. Under such minimal effect conditions, the downstream location is generally favoured, due to the reduced risk of deposition of solid products on the plasma-confinement tube wall.

4.2. Hot-wall conditions

Based on the results obtained for the cold-wall condition, the control of NH_4Cl formation/collection is a very important parameter in developing a single-step synthesis process not involving the use of heat treatment of the powder products. Therefore, this part of this study discusses the use of the hot wall to achieve this goal. Coincidentally, the experimental scheme of hot-wall conditions permitted the study of the effect of (a) variation of reactants ($SiCl_4$ and NH_3) feed rates, (b) location of probe position, (c) plasma plate power, and (d) the presence of carrier gas.

A total of 11 runs was carried out in which the principal parameter investigated was the variation of the reactants feed rate. A summary of the operating conditions and the physical characteristics of the powders obtained under hot-wall conditions is given in Table V.

The powders obtained in each of these runs were fluffy and ultrafine, ranging in colour between white

and brown. These were subject to systematic analysis with the same techniques as employed in the cold-wall condition. However, some semi-quantitative XRD analyses were performed to obtain the level of Si_3N_4 crystalline phase in the powder products. With optimization of parameters such as plate power, reactants feed rates and carrier gas flows, some Si_3N_4 powders, with a crystalline phase content of over 30% by weight (as α and β-Si_3N_4 in equal amounts) were obtained (run H8). Generally, the crystal phase content obtained with the hot-wall system, is higher than that generated by the cold-wall system. A typical X-ray diffraction pattern for the powder (run H8) is presented in Fig. 6 in which the presence of the α and β-Si_3N_4 is clearly indicated. Also, Fig. 7 shows the EDS analysis (run H8 (R)) which allows identification of the impurities in the powder to be made. The small presence of the chlorine (Cl) peak at 2.63 keV indicates that the conversion of $SiCl_4$ to Si_3N_4 is not complete. However, no quantitative analyses for silicon and nitrogen were available to permit calculation of the

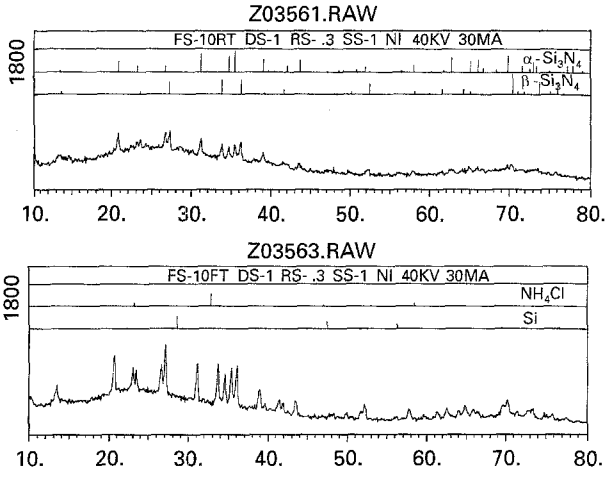

Figure 6 X-ray diffraction pattern of the powder obtained in run H8.

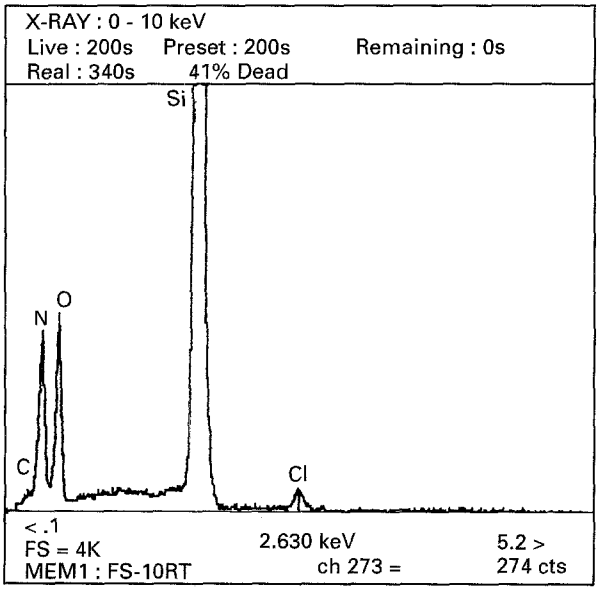

Figure 7 EDS analysis of the powder obtained in run H8 (R).

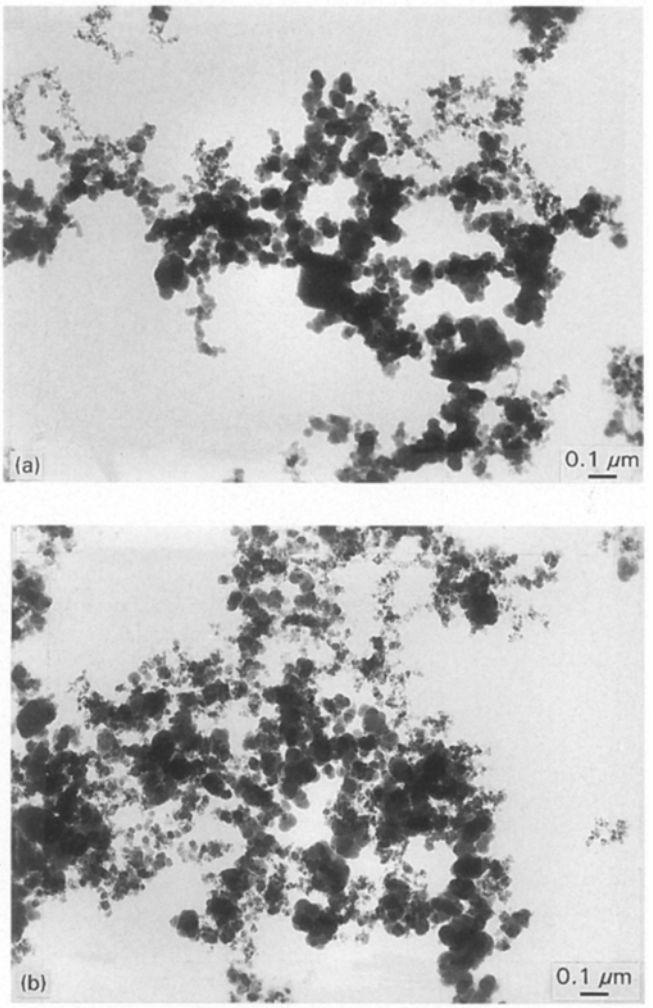

Figure 8 Transmission electron micrographs of the powder obtained in run H8: (a) reactor, (b) filter.

conversion. Finally, typical transmission electron micrographs are given in Fig. 8 (run H8, (a) reactor (b) filter). The photos confirm the morphology and the sizes of the particles.

As shown in Table V, under hot-wall conditions, the NH_4Cl content of the powder was found to vary between 0.7 and 65.0 wt%. Contrary to the cold-wall process observations, the powder from the hot-wall operations generally showed a lower NH_4Cl content in the reactor (R) product than that found in the filter (F) material. Under appropriate hot-wall conditions, it was possible to reduce the powder NH_4Cl content to below 1% by weight (run H6). With the same $NH_3/SiCl_4$ molar ratio, the hot-wall system condensed about 10% of the total NH_4Cl produced in the reaction, while the cold-wall runs condensed more than 30%. These results indicate that the NH_4Cl by-product formation reaction can be controlled by the appropriate wall temperature and reactor design which avoids all cold regions. In this case, graphite was used to produce the hot wall because it was cheap and easy to shape. A better control of wall temperature can be achieved by the use of an appropriate heat transfer fluid such as Dowtherm or Syltherm, but this solution needs more capital investment.

TABLE V Summary of the experimental conditions related to the physical characteristics of the powders obtained from hot-wall configuration

Run	Gas flowrates		Plate power (KW)	feed rate $SiCl_4$ (g min^{-1})	feed rate NH_3 (g min^{-1})	$NH_3/SiCl_4$ molar ratio	Collected powder colour	NH_4Cl (wt %)	Crystal structure	BET specific surface (m^2 g^{-1})	TEM diameter (nm)
	Sheath (standard l min^{-1})	Central (standard l min^{-1})									
H1-R	89 Ar +	59 Ar	25.9	19.8	20.0	10.1	Cream	8.6	Amorph. + α + β < 5%	34.9	47
F	9.6 H_2						Cream	9.1	Amorph. + α + β < 5%	47.6	31
H2-R	89 Ar +	59 Ar	25.9	14.9	16.0	10.7	Cream	11.9	Amorph. + α + β < 5%	38.2	16–47
F	9.6 H_2						Grey	10.6	Amorph. + α + β < 10%	34.2	16–47
H3-R	89 Ar +	59 Ar	25.5	16.6	15.9	9.6	Cream	8.1	Amorphous	30.1	16–78
F	9.6 H_2						Grey	11.0	Amorph. + α + β < 1%	49.7	16–47
H4-R	89 Ar +	59 Ar	25.5	13.3	25.5	19.2	Cream	9	Amorphous	37.4	16–47
F	9.6 H_2						Grey	19.5	Amorphous	47.1	16–31
H5-R	89Ar +	59 Ar	25.9	13.9	13.5	9.7	Cream	4.4	Amorphous	63.2	16–47
F	9.6 H_2						Brown	12.0	Amorphous	85.9	16–31
H6-R	89 Ar +	59 Ar	35.0	17.0	17.7	10.1	White	0.7	Amorphous	59.1	16–141
F	9.6 H_2						Grey	25.1	Amorphous	110.4	8–141
H7-R	89 Ar +	59 Ar	30.3	13.4	17.0	12.7	Brown	16.0[a]	Amorphous + trace Si	20.9	16–47
F	9.6 H_2						Grey	17.4[a]	Amorphous	18.0	16–235
H8-R	89 Ar +	59 Ar	26.6	16.9	18.0	10.6	Brown	16.4	Amorph. + α + β < 10%	39.4	31 + whiskers
F	9.6 H_2						Cream	7.1	Amorph. + α + β < 15%	27.6	31–160 + whiskers
H9-R	89 Ar +	59 Ar	26.6	16.6	26.0	15.6	White	8.7	Amorphous + NH_4Cl	38.7	16–94
F	9.6 H_2						White	65.0	Amorphous	49.7	16
H10-R	89 Ar +	59 Ar	26.6	17.4	16.5	9.5	Cream	14.9	Amorph. + α + β < 1%	52.1	9
F	9.6 H_2						Cream	23.6	Amorph. + α + β < 1%	51.0	16
H11-R	89 Ar +	59 Ar	30.3	16.3	16.0	9.8	Brown	22.4	Amorph. + α + β < 5%	37.8	16
F	9.6 H_2						Cream	18.8	Amorph. + α + β < 10%	31.2	31–78 + whiskers

[a] Reactive powder.

4.2.1. Effect of reactants load

Runs H1 and H2 show clearly that when reactants feed rates are high, the crystalline content of the Si_3N_4 product is low, at a plate power (of 25 kW) and an $SiCl_4$ probe position 78 mm above the outlet of the torch. This result is explained by the temperature drop in the gas mixing zone because of the reactants load effect. Similar runs (H3 and H5) were conducted to study the effect of decreasing the reactants load with a lower $NH_3/SiCl_4$ molar ratio (9.7 instead of 10.7). The resultant products show a colour change in which the amorphous powders produced were browner. These two runs confirm that not only is close control of the reactants feed rate necessary to obtain the right mixing conditions (an adequate feed rate of NH_3 to penetrate the plasma at the desired $NH_3/SiCl_4$ molar ratio), but to also obtain the correct temperature range for best decomposition of the reactants. The results of this study indicate that it is also necessary to obtain information about the plasma reaction concentration and temperature profiles for better control of the reaction yields.

4.2.2. Effect of $SiCl_4$ probe position

The higher probe position (83 mm instead of 78 mm above the outlet of the torch) was examined with a view to reducing the heat losses by the water-cooled probe from 3.4 kW to 3.0 kW without encouraging powder deposition on the ceramic plasma confinement tube. In this probe position, more energy is available to decompose the reactants. This probe position was adopted for the other runs performed in the hot-wall condition.

4.2.3. Effect of NH_3 feed rate

In to this experiment, runs H3 and H4 were carried out to determine the effect of increasing the $NH_3/SiCl_4$ molar ratio of the reactants on the Si_3N_4 powder obtained. These runs showed that, as observed for the cold-wall condition, the free NH_4Cl content of the powder increased with increasing $NH_3/SiCl_4$ molar ratios. Thus, the higher partial pressure of NH_3, combined with the higher overall flowrate to produce a temperature drop in the plasma and thus promote the formation of the NH_4Cl. At a constant $SiCl_4$ feed rate (16.7 g min^{-1}) and plate power (26.6 kW), runs H8 and H9 confirm definitely that a $NH_3/SiCl_4$ molar ratio of around 10 generates a higher crystalline phase content product and minimizes the production of NH_4Cl. Run H8 demonstrates the best conditions found to obtain the most crystalline Si_3N_4 phase and the highest overall Si_3N_4 yield which are both objectives of this work.

4.2.4. Effect of plasma plate power

Runs H6 and H7 were performed at high plate powers (above 30 kW). The results were slightly different; the powders were greyer in colour, with a trace of silicon and were also difficult to characterize. This powder produced white fumes in contact with air and was considered reactive (run H7) because of unreacted $SiCl_4$. This behaviour is explained by the increase in temperature which permits total NH_3 decomposition in nitrogen which decreases the reactivity of the chemical system. So, the chlorosilanes (reactive with air) condense after gas quenching, in the powders because they cannot react with nitrogen. These results tend to confirm the higher reactivity of the NH radicals in comparison to atomic nitrogen. Run H11 in comparison with run H5 shows that this system is very sensitive to small changes of plate power (30.3 kW to 25.9 kW) and small variations in the $SiCl_4$ feed rate (16.3 g min^{-1} to 13.9 g min^{-1}) at a constant $NH_3/SiCl_4$ molar ratio of 9.8, because the powder structure was more crystalline in the case of a higher plate power and higher $SiCl_4$ feed rate (run H11). Thus, the system has a narrow temperature range in which the correct reaction may be obtained, involving the correct excess of NH_3, etc.

All of these runs show that is difficult to achieve the decomposition of NH_3 simultaneously with the formation of the nitride. At higher temperatures, which is the case at high plate powers, reformation of nitrogen reduces the kinetics of the Si_3N_4 synthesis, while at low temperature the kinetics themselves are limiting.

4.2.5. Effect of NH_3 carrier gas

Run H10, which used 5 standard l min^{-1} argon to increase the injection velocity of the NH_3 feed in comparison to run H8 produced more of the amorphous powder. This result is explained by the temperature drop which also affects the kinetics of Si_3N_4 formation. This result indicates that it is better to control the injection velocity by modifying the geometry of the injection ports, e.g. smaller injection port diameter, rather than dilute the reactants with an inert gas.

5. Conclusions

The present study has demonstrated the feasibility of plasma synthesis of ultrafine crystalline Si_3N_4 powder through the gas-phase reaction of $SiCl_4$ and NH_3 in an inductively coupled r.f. plasma. The effect of the reactor wall temperature was clearly observed. The cold-wall reactor produced powders of greater amorphous phase content and a considerable amount of NH_4Cl which could be eliminated by product heat treatment. In this configuration, the Si_3N_4 BET determined specific surface area was around 60 m^2 g^{-1}. The use of the hot-wall reactor considerably reduced the product NH_4Cl content (to < 1 wt %) and produced a more crystalline powder as α and β-phase Si_3N_4 in equal amounts (total > 30 wt %). The powder BET specific surface area was reduced to around 40 m^2 g^{-1}. Some process improvements, e.g. the use of a high-temperature heat-transfer fluid heated reactor, instead of graphite sleeves would permit the operation of a satisfactory single-step process for Si_3N_4 powder

production. Many operating conditions such as the $SiCl_4$ probe position, plasma plate power, quench gas flowrate, carrier gas flowrate, plasma sheath gas composition and reactants feed rate all influence the quality of the resultant powder. $NH_3/SiCl_4$ reactants fed at molar ratios below 10, produce the more crystalline powders.

Finally, the desired chemical reaction is strongly dependent on the maintenance of a narrow reaction temperature range; at high temperatures (high power), the reformation of nitrogen reduces the kinetics of the reaction; at low temperatures, the kinetics themselves are limiting. Therefore, to improve the product yields and properties of this reaction, developments in on-line diagnostics, for temperature and concentration pattern control, will be necessary.

Acknowledgements

The authors gratefully acknowledge the financial support of the Conseil de Recherche en Sciences Naturelles et en Génie Du Canada (CRSNG), the Fonds pour la Formation de Chercheurs et l'Aide la Recherche (FCAR) and the Canadian Electrical Association (CEA).

References

1. Hains Technology Associate and MKM Consultants International, "Impact of Advanced Ceramics on Ontario Industry", Ontario Ministry of Northern Development and Mines, Industrial Mineral Background Paper 9 (1988) 96 pp.
2. L. M. SHEPPARD, *Am. Ceram. Soc. Bull.* **68** (1989) 979.
3. C. B. LAFLAMME, G. SOUCY, J. JUREWICZ and M. I. BOULOS, *J. High Temp. Chem. Process.* **1** (1992) 283.
4. T. TSUTSUMI, in "Silicon Nitride-1" Vol. 1, edited by S. Somiya, M. Mitomo and M. Yoshimura, Ceramic Research and Development in Japan (Elsevier Science, New York, 1990) pp. 13–23.
5. H. W. RHODES and S. NATANSOHN, *Am. Ceram. Soc. Bull.* **68** (1989) 1804.
6. T. ISHII, A. SANO and I. IMAI, in "Silicon Nitride-1", Vol. 1, edited by S. Somiya, M. Mitomo and M. Yoshimura, Ceramic Research and Development in Japan (Elsevier Science, New York, 1990) pp. 59–69.
7. Y. KOHTOKU, *ibid.* pp. 71–80.
8. K. NAKAGAMA and M. KATO, *ibid.* pp. 25–37.
9. T. ARAKAWA, *ibid.* pp. 81–92.
10. M. NAKAMURA, Y. KURANARI and Y. IMAMURA, *ibid.* pp. 39–58.
11. T. HUSSAIN and V. J. IBBERSON, in the "7th International Symposium on Plasma Chemistry", Symposium Proceedings edited by C. S. Timmermans, Eindhoven, The Netherlands; 1–5 July, 1985 (IUPAC Subcommittee of Plasma Chemistry) Eindhoven, Vol. 2 (1985) pp. 692–96.
12. R. LI and W. GU, in "Production and Processing of Fine Particles", Proceedings of the International Symposium on the Production and Processing of Fine Particles, edited by A. S. Plumpton from Centre de recherche minérales, Saint Foy, Montreal, Québec, Canada. August 28–31, 1988. © The Canadian Institute of Mining and Metallurgy (Pergamon Press, New York, USA) pp. 559–68.
13. J. SZÉPVÖLGYI, I. TÓTH and T. SZÉKELY, *Collo. Phys.* (C5) *suppl. J. Phys.* **51** (18) (1990) C5–35.
14. T. YOSHIDA, H. ENDO, K. SAITO and K. AKASHI, in, "6th International Symposium on Plasma Chemistry", Symposium Proceedings edited by M. I. Boulos and R. J. Munz, Montréal, Québec, Canada, IUPAC Subcommittee of Plasma Chemistry, Vol. 1, 24–28 July 1983, p. 225.
15. H. J. LEE, K. EGUCHI and T. YOSHIDA, *J. Amer. Ceram. Soc.* **73**(11) (1990) 3356.
16. L. M. SHEPPARD, *Am. Ceram. Soc. Bull.* **70**(4) (1991) 692.
17. G. LANTAGNE, B. MARCOS and B. CAYROL, *Comput. Chem. Eng.* **12** (1988) 589.
18. M. W. CHASE, C. A. DAVIES, J. R. DOWNEX, D. J. FRURIP, R. A. McDONALD and A. N. SYVERUD, *J. Phys. Chem. Ref. Data* **14** suppl. 1 (1985) 1856.
19. M. E. COLTRIN, R. J. KEE and J. A. MILLER, *J. Electrochem. Soc. Solid State Sci. Technol.* **131** (1984) 425.
20. G. SOUCY, J. W. JUREWICZ and M. I. BOULOS, *Plasma Chem. Plasma Process.* **14** (1994) 43.
21. *Idem, ibid.* **14** (1994) 59.
22. *Idem, ibid.* (1994).
23. G. SOUCY, PhD thesis, Chemical Engineering Department, Université de Sherbrooke, Sherbrooke, Québec (1992) 234 pp.
24. D. S. PHILLIPS and G. J. VOGT, *Mater. Res. Soc. Bull.* **12** (1987) 54.

Received 15 February
and accepted 4 October 1994